



Received September XX, 2020; revised; accepted October XX, 2020; Date of publication November XX, 2020; date of current version November XX, 2020.

Digital Object Identifier 10.1109/JMW.2020.Doi Number

Millimeter-Wave Imaging at 652 Frames per Second

STAVROS VAKALIS¹ (Student Member, IEEE), DANIEL CHEN¹ (Student Member, IEEE), AND JEFFREY A. NANZER¹ (Senior Member, IEEE)

¹Electrical and Computer Engineering, Michigan State University, East Lansing, MI, 48824, USA.

CORRESPONDING AUTHORS: Stavros Vakalis (e-mail: vakaliss@msu.edu), Jeffrey A. Nanzer (e-mail: nanzer@msu.edu)

This work was supported by the National Science Foundation under Grant ECCS-1708820.

ABSTRACT Millimeter-wave technology has the potential to revolutionize the field of electronic imaging due to the ability to generate images with high resolution through obscurants like fog and smoke or through materials such as garments and baggage. While millimeter-wave technology has become smaller and more commercially viable in recent years, existing millimeter-wave imaging approaches have been limited by image acquisition time, inhibiting their wide adoption. In this work, we demonstrate a new method of millimeter-wave imaging that uses the transmission of noise signals paired with an element-level 38 GHz digital receiving array to generate millimeter-wave imagery at 652 frames per second. Using a new parallel data acquisition and image formation approach, latencies were reduced by a factor of nearly 50 compared to the authors' prior work, yielding frame rates more than 26 times faster than any other reported millimeter-wave imaging system. Such imaging capability significantly expands the opportunities for millimeter-wave commercial and scientific imaging applications including contraband detection, consumer sensing, industrial imaging, and nondestructive evaluation. We discuss the millimeter-wave hardware architecture, the imaging algorithm, and present experimental high-speed millimeter-wave imagery.

INDEX TERMS Digital arrays, high-speed imaging, interferometry, millimeter-wave imaging, noise signals.

I. INTRODUCTION

Imaging is crucial in scientific and consumer applications due to the high information density of images and the human ability to rapidly interpret image data. While imaging at infrared, optical, and higher frequencies has a long history, imaging in the millimeter-wave region of the electromagnetic spectrum, extending from 30 GHz to 300 GHz (wavelengths from 10 mm to 1 mm), has only recently begun to be explored in earnest and thus holds particular interest. Over the past couple decades, millimeter-wave imaging has been used for long-range remote sensing applications [1], [2], and more recently has been used in shorter-range scenarios such as security sensing (e.g. [3], [4]). Millimeter-wave electromagnetic signals have unique properties making them ideal for a wide range of challenging applications beyond traditional remote sensing. Wavelengths in this spectrum are not only sufficiently small that high-resolution images of common objects can be formed, but are also sufficiently long that they can easily propagate through a wide range of media that would inhibit other imaging modalities. Millimeter-wave signals penetrate through obscurant conditions such as fog and smoke with negligible attenuation, enabling sensing in a wide variety of environmental conditions [5]. Millimeterwaves can also propagate through most garment and baggage material without significant loss, supporting the detection of contraband [6]. At lower microwave frequencies, medical imaging applications are also possible [7], [8]. Furthermore, since millimeter-wave radiation is non-ionizing, it is safer to operate in the presence of humans or other living organisms in comparison to higher energy imaging modalities like Xrays. The differing interactions of millimeter-wave signals with varying material properties also make them useful for industrial imaging and non-destructive evaluation [9], [10], [11].

1

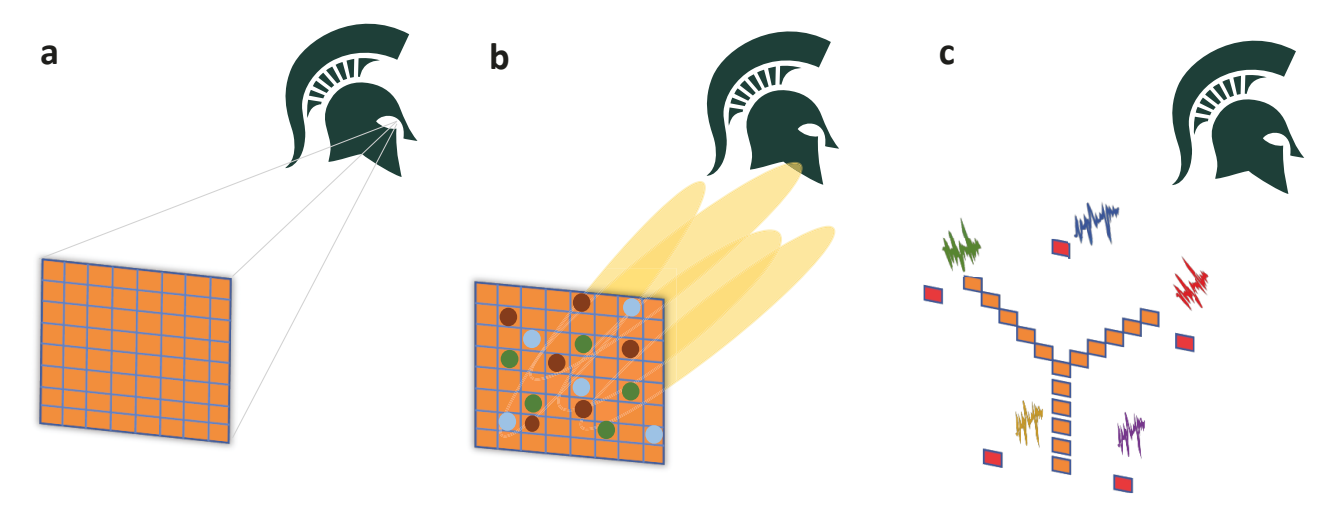


FIGURE 1. Millimeter-wave imaging approaches. (a) Conventional imaging systems use a focused beam that scans over the image plane to sequentially build up an image. (b) Computational imaging systems use coherent pseudo-random illumination, but require accurate knowledge of the transmitted signals and resultant space-time illumination of the scene. (c) The presented incoherent imaging system uses a sparse receive array and incoherent noise illumination, where the transmit signal does not need to be known precisely; only the transmit signal statistics need to be known.

Despite the great potential of millimeter-wave imaging applications, the adoption of millimeter-wave technology has been hindered by fundamental limitations in existing imaging approaches. Principal among these is the limitation on acquisition time, which has made video-rate millimeter-wave imaging challenging to achieve. Another fundamental limitation is the requirement for a large antenna aperture to obtain high-resolution capability.

Existing millimeter-wave imaging systems can be categorized as either coherent active imagers or incoherent passive imagers. Active imaging systems rely on the transmission of a known signal that scatters off the scene and is captured by a receiving antenna. In order to form an image, coherent active systems must scan a narrow beam either mechanically or electronically using a larger antenna with a mechanical gimbal or a phased array [12], [13], [14], [15]. Both mechanical and electrical scanning approaches are limited by their scan time, and require a large antenna aperture. Recent developments in computational microwave imaging have managed to reduce the number of components and data acquisition time [16], [17]. However, the trade-offs manifest through increased image reconstruction time which requires solving a computationally expensive inverse problem.

In contrast, incoherent passive millimeter-wave imagers do not rely on an active transmission and capture signal emissions from the environment's radiation [18], [19], [20]. Thus, these systems can use Fourier-domain imaging techniques that rely on the reception of signals that are spatially and temporally incoherent and can be implemented in sparse arrays with significantly reduced receive aperture area, as described in the Van Cittert-Zernike theorem [21], [22]. The theorem suggests that for a spatially incoherent source, its spatial Fourier transform can be reconstructed using coherence measurements. However, the signals that are captured are generated thermally by the scene and are exceedingly low

in power, necessitating very high signal amplification and processing gain [3]. These requirements generally translate to both high cost and long integration times, considerably limiting fast image acquisition capabilities. Few previous works have demonstrated millimeter-wave image formation for passive objects at speeds close to video-rate, with the fastest reported image formation of passive objects for 25 frames per second (fps) [23], less than half of traditional optical video rates.

Through a new combination of active and passive sensing techniques, we have developed a 38 GHz imaging system producing millimeter-wave imagery at 652 fps in real time. We base the system on a novel concept of active incoherent imaging, where the imager transmits incoherent noise signals, thereby satisfying the Van Cittert-Zernike theorem requirements. The use of noise signals is inspired from noise radar [24], [25], [26]; however, while noise radar generally requires exact knowledge of the transmitted noise waveform to support coherent processing, active incoherent imaging requires only knowledge of the waveform statistics, significantly easing the waveform characterization process. The use of Fourier-domain imaging can take place using a sparse receive array with aperture area an order of magnitude smaller than traditional filled apertures. When combining the noise illumination with an element-level digital array receiver, images of passive objects can be obtained with low latency. In previous work, we have discussed the concept of using noise signals for incoherent imaging [27], and the design considerations and experimental measurements for a millimeter-wave interferometric antenna array [28]. In this work, we discuss and experimentally demonstrate the capability to generate images rapidly, at frame rates orders of magnitude faster than existing active approaches. This significant increase in millimeter-wave imaging speed holds considerable promise for a number of scientific and





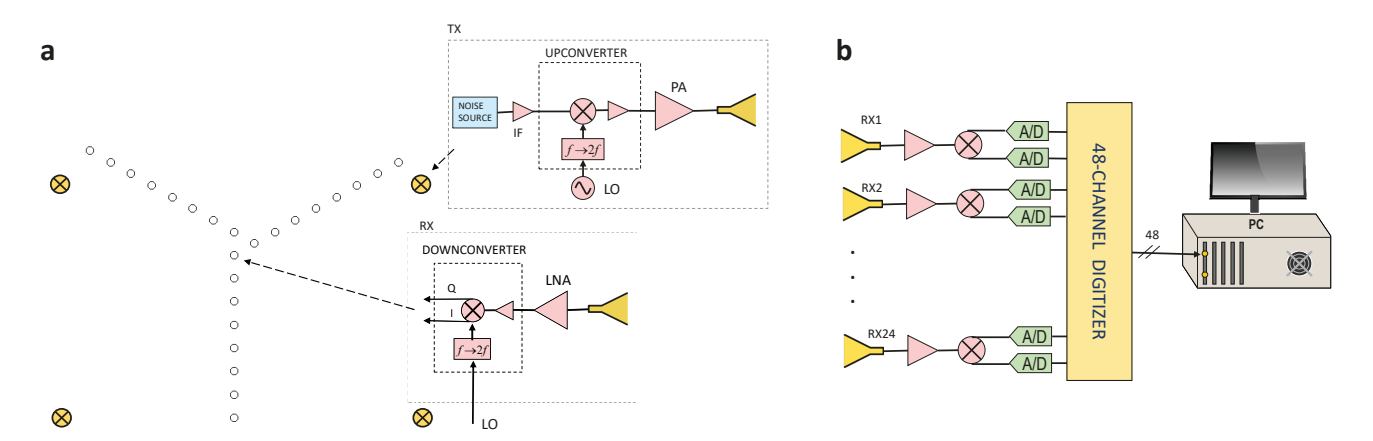


FIGURE 2. (a) Interferometric imaging system architecture; 24 receivers (represented by white circles) are located in the locations of a Y-array and 4 transmitters (represented by the yellow circles with crosses) are placed just outside the receiving array. (b) Simplified digital array architecture used in this work. The receive waveforms are quadrature downconverted and then captured by three 16-channel digitizers (48 channels in total) hosted in a computer.

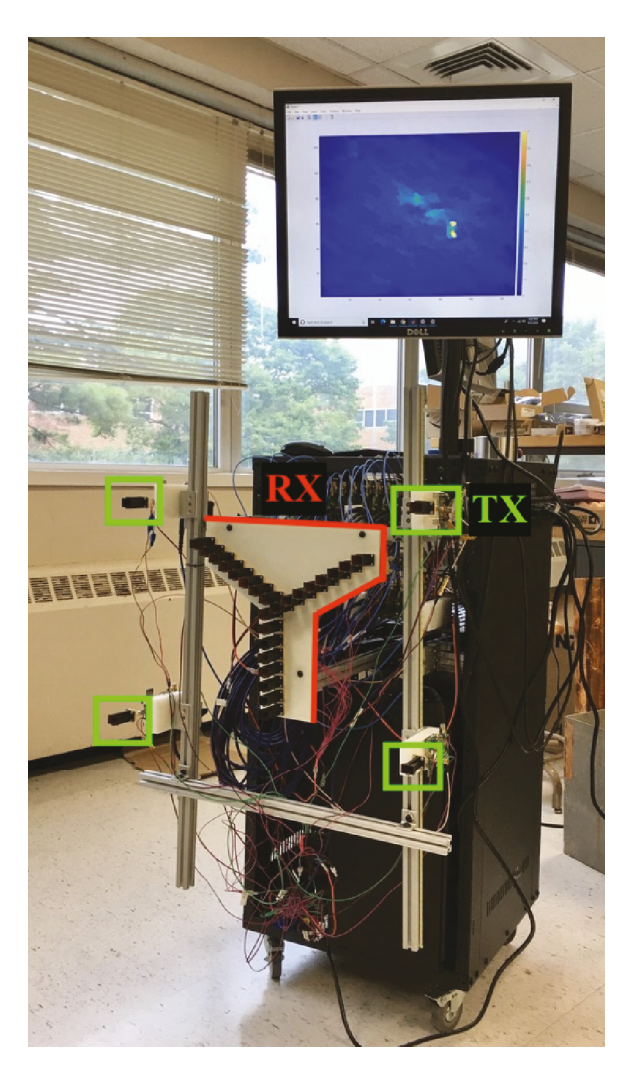


FIGURE 3. Photograph of the millimeter-wave imaging system. The transmitters are shown in the green boxes, while the receive array is outlined with red. The millimeter-wave hardware, power supplies, digital hardware, and computer are hosted inside the rack.

commercial applications, such as dramatically faster security screening in airports, where large crowds of people can be screened in high-speed, rapid defect detection in industrial processes and fast-moving production belt lines, and high-accuracy imaging of fast moving objects, which cannot be tackled by techniques such as synthetic aperture radar [29], among others.

Previously, we demonstrated a 16-element active incoherent millimeter-wave imaging system that obtained images at 13.7 fps using serial data acquisition and image formation [30]. In this work, we significantly expand this system by developing an element-level digital millimeterwave imager with 24 elements that overcomes a significant bottleneck in the image formation process by implementing a parallel data acquisition and image formation approach. By allowing the data acquisition to take place in parallel to the image formation algorithm, significant latencies associated with repeated initialization and termination of the acquisition process are eliminated during real-time operation. Furthermore, data can continue to be acquired while images are generated. The result is a significant reduction in processing latency, yielding an increase in frame rate of nearly 50 times to a rate of at 652 fps, which is orders of magnitude larger than current state of the art in millimeter-wave imaging.

II. ACTIVE INCOHERENT MILLIMETER-WAVE IMAGING

Most current active millimeter-wave imaging techniques can be grouped into two categories: scanning systems such as mechanically or electronically-steered arrays (Fig. 1(a)), and computational millimeter-wave imaging systems (Fig. 1(b)). Scanning techniques employ some form of mechanical movement or electrical focusing of the diffraction-limited beam of an aperture. The temporal bottleneck is the required physical scan time; while electronic steering mitigates this, it comes at the expense of increased hardware complexity and greater cost. A significant improvement on shortening the data acquisition time and reducing the number of active

components can be achieved by using computational imaging. Using coded apertures, measurement modes from the scene reflections can be obtained without scanning. However, these techniques are prone to the need for solving an inverse problem of a set of linear equations $\mathbf{y} = \mathbf{A}\mathbf{x}$, where \mathbf{y} corresponds to the measurement samples, \mathbf{A} is the sensing matrix, and \mathbf{x} is the imaging scene. This problem can be computationally expensive and time consuming. Although the data acquisition time of computational techniques is shorter than scanning techniques, it is still not sufficiently fast for high-speed imaging due to the need to sweep over a large enough bandwidth or switching between measurement modes [31]. In both cases, a large filled aperture is generally required. For high-resolution imagery, the result is a bulky and expensive aperture.

Active incoherent millimeter-wave imaging supports faster image formation with an aperture area an order of magnitude smaller than traditional filled apertures. The approach is based on the use of an incoherent transmitted signal that yields a scattered electromagnetic field that is uncorrelated in space and time. Image reconstruction is supported through sampling the Fourier-domain information, as described by the Van Cittert-Zernike theorem [21], [22]. Current interferometric millimeter-wave systems employ passive radiometric receivers capturing thermal emissions, which, due to their inherent random nature, satisfy the Van Cittert-Zernike theorem requirements. However, the thermal signals from terrestrial objects in the millimeter-wave band have signal powers on the order of picowatts or less [3], requiring significant receiver sensitivity, which is addressed through high gain receivers and long integration times. Recently, we introduced and demonstrated a method of transmitting incoherent signals from multiple locations to mimic thermal radiation, which allows the use of Fourier domain sampling without the sensitivity requirements of passive systems [27], [28].

Fourier domain sampling enables the use of sparse antenna apertures with 10% or fewer elements than a traditional phased array. The high signal power resulting from active incoherent transmission enables the system to operate with receive gains on the order of 20-30 dB, significantly less than the 100+ dB gain typically required for passive imagers. These two aspects are critical for fast image formation time, since they significantly reduce the necessary integration time, and can form images without beam-scanning [32], [33]. Furthermore, in contrast to other computational imaging techniques, no precise knowledge of the transmit waveform is necessary; only the transmitted signal statistics need to be known to ensure the signals are spatially and temporally incoherent at resolution level of the system. As shown in Fig. 1(c), the incoherent millimeter-wave imaging system illuminates the scene from multiple locations using noise transmitters (shown as red rectangles) and performs image formation by cross-correlations on a sparse receiving interferometric antenna array (shown as orange rectangles)

[32], [34]. The pairwise cross-correlations sample the spatial Fourier transform of the scene, which is called the scene visibility $\mathcal{V}(u,v)$, where u and v are spatial frequencies. This process is usually referred to as spatial frequency sampling and is significantly different from typical imaging techniques that collect samples in the spatial domain. Unlike a scanning technique, which focuses the energy in the spatial domain on a specific pixel at every capture, all elements in interferometric arrays simultaneously capture information that corresponds to the entire scene. Interferometric arrays operate similarly with a camera with global shutter, thereby providing a mechanism to significantly reduce the data acquisition time and motion blur. The reconstructed scene intensity I_r is obtained from the visibility samples \mathcal{V}_s through an inverse Fourier transform

$$I_r(\alpha, \beta) = \iint_{-\infty}^{\infty} \mathcal{V}_s(u, v) e^{-j2\pi(u\alpha + v\beta)} dudv \qquad (1)$$

where α, β are the direction cosines relative to the two spatial frequencies u, v.

Interferometric image reconstruction is efficient because there is minimal coupling between the response at each spatial point and therefore there is no need to decode the data afterwards. This is not the case in computational imaging approaches which require the solution of an inverse problem. In essence, this means that every point in the scene should behave like an independent radiator. To support this, active incoherent millimeter-wave imaging uses the transmission of noise signals to illuminate the scene. Using noise transmission from multiple locations, this approach imposes low spatial coherence in the scene, supporting image reconstruction using (1) [35].

Image formation time is closely tied to the sensitivity of a Fourier domain imager. The radiometric sensitivity ΔT of such a receiver is inversely proportional to the square root of the system bandwidth B and integration time τ by

$$\Delta T = C \frac{T_{sys}}{\sqrt{B\tau}} \tag{2}$$

where T_{sys} is the system noise temperature and C is a constant that depends on the receiver configuration [1], [3]. Because thermal radiation is exceedingly low in power at millimeter-wave frequencies, passive systems with high gain still require observation bandwidths of hundreds of MHz or more, and necessitate integration times from milliseconds up to seconds [36], [37]. Even high speed optical cameras do not operate well under low light conditions because of the necessary integration time to obtain reasonable image sensitivity. In contrast, active incoherent millimeter-wave imaging significantly increases the received signal power, enabling the use of very short integration times. Using data acquisition devices with sampling rates in the order of MS/s, we can achieve receiver time-bandwidth products [38] on the order of 1000 or more with integration times on the order of μ s, which are sufficient for interferometric image formation. This integration time is orders of magnitude shorter than that





of typical passive millimeter-wave imaging systems, and at least one order of magnitude shorter than most computational microwave imaging techniques [16].

III. HARDWARE AND SOFTWARE ARCHITECTURE

The system diagram is shown in Fig. 2. The imager employs four noise transmitters placed outside the receiving array, and 24 receivers shaped in a Y configuration, which are shown in Fig. 2(a). The receiving array shape plays a significant role in the amount of spatial frequency information that is sampled by the system [39]; the Y shape was chosen because of the high density of its spatial sampling function [40]. Each received signal is downconverted to baseband and sampled by a high-speed digitizer. The millimeter-wave receiving array is element-level digital, meaning that all processing of the signals received at each element occurs in the digital domain; this is in contrast to traditional phased arrays, where analog signal combination before sampling is typical. A simplified diagram of the digital array is shown in Fig. 2(b). The use of active illumination decreases the integration time and bandwidth compared to passive systems, thus the image reconstruction algorithms can be run quickly in the time-domain using multi-channel digitizers and a consumer-grade computer, without the need for dedicated processing hardware like field programmable gate arrays (FPGAs) [30]. Furthermore, the reconstruction algorithm does not require an iterative solver or computationally expensive matrix inversions found in computational imaging techniques. A photograph of the imager can be seen in Fig.

A. Millimeter-wave hardware architecture

The 38 GHz digital millimeter-wave imager consisted of 24 receiving elements and 4 transmitting elements. The 24 receivers (RX) were placed in a Y-array formation [40], and the spacings between neighboring receive antenna elements was 24 mm (3.04 λ). The half-angle unambiguous field of view of an interferometric imager with element spacings d_x and d_y across the horizontal and vertical axes can be expressed for the two direction cosines α and β as

$$FOV_{\frac{\alpha}{2},\frac{\beta}{2}} = \frac{\lambda}{2 \cdot d_{x,y}} \quad . \tag{3}$$

The unambiguous field of view of the imager is 22° and 41° in the azimuth and elevation planes, respectively. The resolution of the imager in the azimuth and elevation planes can be approximated with the null-to-null beamwidth θ_{NNBW} of the fringe response from the largest baselines in the horizontal and vertical axes of the array x and y. This can be defined as

$$\Delta\theta_{\alpha,\beta} \approx \theta^{(\alpha,\beta)}_{NNBW} \approx 2 \frac{\lambda}{D_{x,y}}$$
 (4)

The maximum antenna separation in the horizontal and vertical axes of the array were $D_x = 31.2$ cm and $D_y = 27.6$ cm. The imager has a spatial resolution of 2.9° and 3.3° in the azimuth and elevation planes, respectively.

The 3D-printed receive antenna holding structure had horizontal and vertical dimensions of 34 cm and 34 cm respectively. The 4 transmitters (TX) were separated at horizontal and vertical spacing of 56 cm and 49 cm, respectively. The noise transmitters consisted of 0.1-2 GHz calibrated noise sources with 15 dB excess noise ratio (ENR), that were upconverted to 38 GHz using Analog Devices (ADI) HMC6787A upconverters. At 38 GHz the noise signals were amplified using ADI HMC7229 power amplifiers, feeding approximately -10 dBm of power into every transmit antenna. Both transmitters and receivers utilized 15 dBi 3Dprinted horn antennas that were fabricated at Michigan State University. Consequently, every transmitter had an Effective Isotropic Radiated Power (EIRP) of 5 dBm. Because all four transmitters are incoherent with each other, the total EIRP of the imaging system can be approximated as 5 dBm + 6 dB = 11 dBm. For the receivers, each antenna was followed by a 20 dB gain ADI HMC1040 low-noise amplifier (LNA) before being downconverted to baseband using an ADI HMC6789 I/Q downconverter. The same 19 GHz local oscillator (LO) was used for all the downconverters after being split into 24 ways.

B. Digital hardware and software architecture

The downconverted signals were captured using three 16channel ATS9416 14 bit, 100 MS/s, AlazarTech waveform digitizers installed on a computer in master-slave mode. The three digitizers had frequency locked clocks and time triggering took place using a common 1 kHz signal in order to make sure that there was no frequency offset or timing jitter between the 48 baseband channels (24 complex signals). The computer had an Intel i9-9820x processor and 64 GB of RAM. The complete imaging system was mounted on a computer rack. The desktop computer was placed at the bottom of the rack while the receive hardware and power supplies were placed on separate shelves. The image reconstruction algorithm was executed in MATLAB. The data buffers of the captured waveforms were processed in parallel while the data acquisition was still running in order to minimize time delays due to acquisition initialization and termination.

In our previous work, the signal processing was implemented in a serial data acquisition and image formation format, as shown in Fig. 4(a) [30]. In this format, the data acquisition is initialized and terminated with each data capture associated with an image. The data is then transferred to a processor where the image formation algorithm is implemented. While this approach is simple to implement, the process of starting and stopping the data acquisition has significant associated latencies that dramatically reduce the overall time between acquisition and image formation, limiting the frame rate. In the system presented here, we implement a new parallel data acquisition and image formation approach that eliminates the most significant latencies involved with the serial approach and allows for future improvement of frame rates. In the parallel processing ap-

VOLUME 00 2020 5

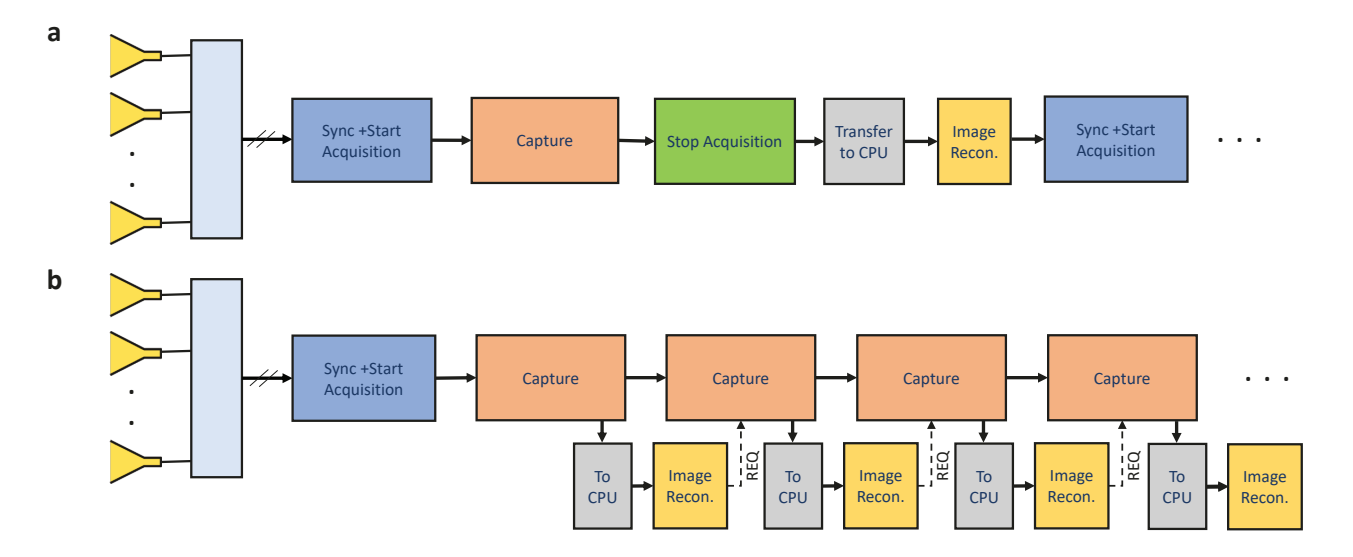


FIGURE 4. Comparison of a serial-based data acquisition and image formation approach and the proposed parallel acquisition and image formation approach. (a) Serial data acquisition and image formation. The Synchronize (Sync) + Start Acquisition and Stop Acquisition steps must take place with each data capture, leading to long latencies. (b) Parallel data acquisition and image formation. The Sync + Start Acquisition process only needs to be implemented once, after which, captures are obtained continuously. In parallel, the data is transferred to a processor for image formation when there is a request (REQ). Once the system is halted, the Stop Acquisition command is implemented only once. In this format, the capture time period (integration time of the noise signals) represents the theoretically limiting factor; a 1 ms integration time thus has a theoretical limit of 1000 fps. In our system, transferring data to the processor and the image formation process consume more time than the capture, yielding 652 fps with a 64 μ s integration time/capture window length. Reducing the transfer latency and image processing time will serve to further increase the frame rate of the system. (Block size in the image is not commensurate with time latency.)

proach, shown in Fig. 4(b), data acquisition is initialized only once at the beginning of the video operation. Data is captured continuously and is transferred to the processor in parallel. During the image formation process, data can still be captured continuously. Once the image formation is complete, the processor requests additional data for the next frame. Data acquisition termination is only implemented once at the end of the video process. The new parallel approach reduces latencies and thus increases the video frame rate through two principal means. First, the timeconsuming initialization and termination processes of the data acquisition are effectively eliminated, as they are only used at the beginning and end of the entire video process, rather than for each data capture. Second, by running the image formation algorithm in parallel to the data capture process, data can be acquired continuously. Theoretically, the limiting latency factor is thus the data observation time, which is commensurate with the capture length. If the data transfer and image formation processes consume less time than the observation time, the system achieves its theoretical maximum frame rate. For example, an observation time of 1 ms would then yield a theoretical maximum frame rate of 1000 fps.

The image reconstruction process, denoted in the yellow box in Fig. 4, is summarized in Fig. 5. The time-domain noise reflections from the scene are captured at the 24 receive antenna locations and the complex signals V(t), each containing an in-phase (I) and quadrature (Q) component, are captured with 48 parallel digitizers. In order to perform

the cross-correlations between all the antenna elements in the array, which in this case is the dot product between every two antenna elements, we multiply V(i,t), which is the complex response of the ith element, with its conjugate transpose. In this way each row of the matrix V(i,t) is multiplied with each column of $V^H(j,t)$, which is the conjugate response of the jth element, and then summed (integrated). Afterwards, the cross-correlations are mapped to visibility samples \mathcal{V}_s based on the antenna pairs generating the samples, and the image is reconstructed through an inverse fast Fourier transform (IFFT). At the right end of Fig. 5, the simulated reconstruction of a H-shaped target is shown.

The integration time in this work was 64 μ s, however the latencies associated with the data transfer and image formation limited the frame rate to 652 fps. The total latency can be estimated as $\frac{1}{652}$ s - 64 μ s = 1.469 ms. This means that the image reconstruction frame rate has still room for improvement by using a higher-speed data bus and an application-specific integrated circuit (ASIC) for the image reconstruction. The millimeter-wave video was not plotted in real-time as the computer display did not have the required refresh rate.

IV. EXPERIMENTAL HIGH SPEED IMAGE RECONSTRUCTIONS

Proof-of-concept experiments were conducted in a semianechoic environment. A pendulum was created by fixing a 50 cm transparent line on a rod hanging from the ceiling. A foam sphere with a 7.6 cm diameter covered in





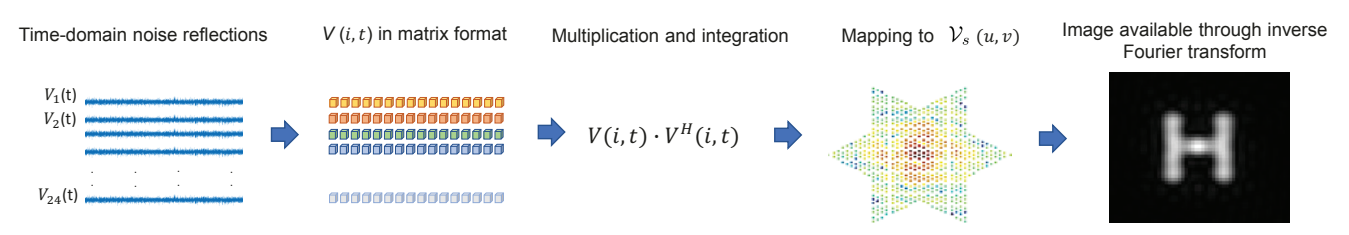


FIGURE 5. Overview of the digital signal processing algorithm. The reflected noise signals from the scene are captured in time domain and create the voltage matrix V(i,t). The voltage matrix is multiplied with its conjugate transpose $V^H(i,t)$, which is a highly optimized operation. Afterwards the cross-correlations are mapped to spatial frequency samples and the image is available through an inverse Fourier transform. [30]

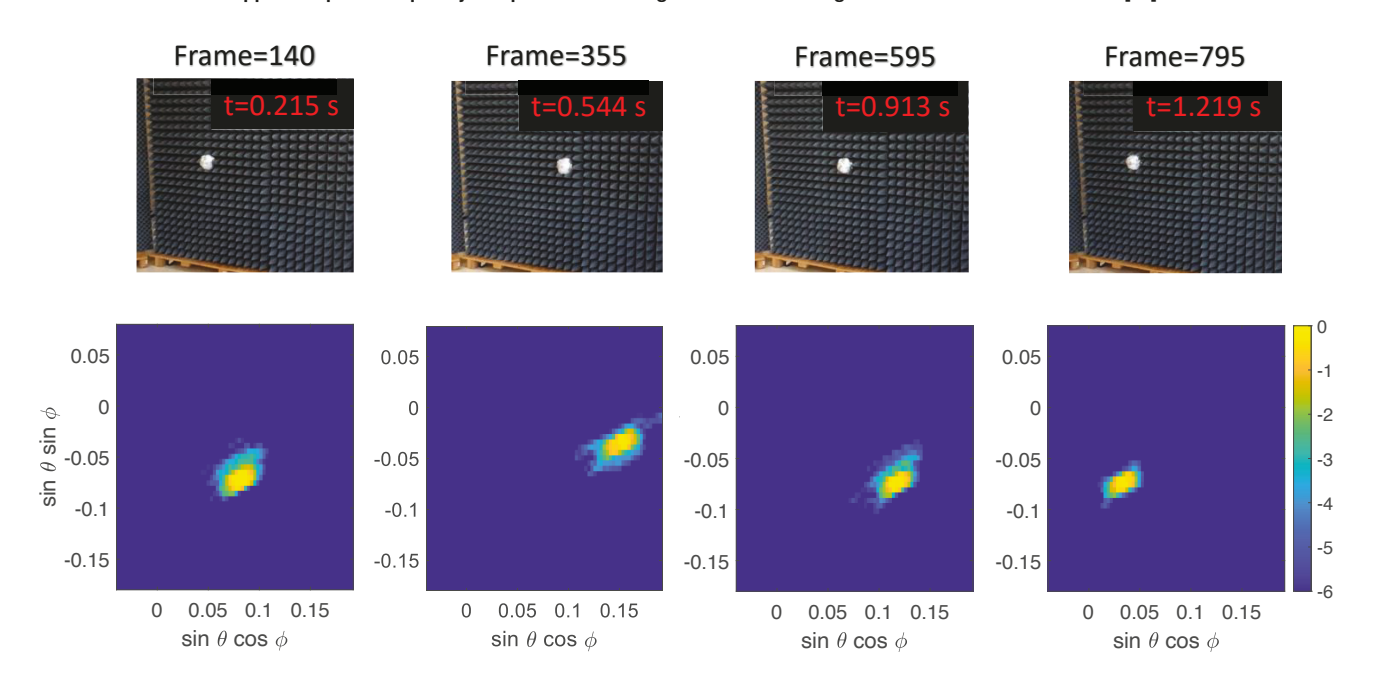


FIGURE 6. High-speed imaging results. Four different frames of the optical video of the pendulum (top) and millimeter-wave image reconstruction (bottom). The colorbar values correspond to the reconstructed image intensity I_r and are in dB. A slow motion video can be found in the supplemental material.

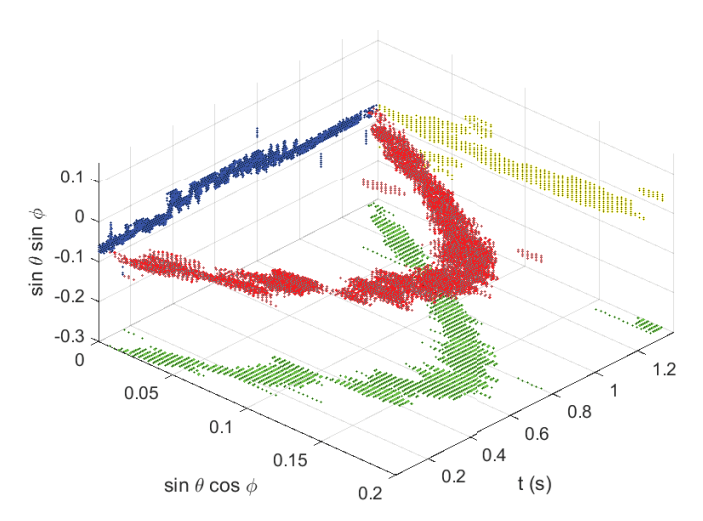


FIGURE 7. Three dimensional plot showing the pendulum movement as a function of the two direction cosines $\sin\theta\cos\phi$ and $\sin\theta\sin\phi$ and time.

aluminum tape was attached at the end of the line. The sphere was allowed to swing on the pendulum across the field of view of the imaging system at a distance of 1.12 m. yielding a received power of -68 dBm at the output of each receive antenna. While a comparison to passive systems is not directly feasible since passive systems detect thermally generated power and not reflected power, a sphere with perfect emissivity of the same size at room temperature emits a thermal power of $P_t = kTB$, where $k = 1.38 \times 10^{-23}$ is the Boltzmann constant, $T=290\ K$ is room temperature, and $B=50~\mathrm{MHz}$ is the maximum bandwidth. The received power can be found via the Friis transmission equation to be equal with -111 dBm at the output of each receiver antenna. This also represents an ideal case, as it assumes perfect emissivity and full use of the receiver bandwidth, but is nonetheless significantly lower than that for the active system, and would require much higher gain for equivalent sensitivity. Note that this is even without consideration of the total integration time; the sensitivity of passive imagers is inversely proportional to the square root of the integration

VOLUME 00 2020 7

time, thus shorter integration times yield larger (worse) sensitivity.

Four time-lapse screenshots of the millimeter-wave image reconstructions of the pendulum sphere and the corresponding optical frames can be seen in Fig. 6. A slow-motion millimeter-wave video capture of the moving pendulum sphere can be found in the supplemental material [41], along with the slow-motion optical video that was captured using an iPhone SE at 240 fps. The slight blurring of the target response is the result of hardware imperfections and also due to the imperfections of the sphere shape: the aluminum tape covering the sphere was not perfectly smooth, thus reflections from the sphere do not appear as an ideal point source. Total variation denoising was used on the millimeterwave images [42]. The experimental imaging frame rate was calculated by using an optical video camera with time stamps as ground truth. These results were also cross-validated with the pendulum oscillation period $T=2\pi\sqrt{\frac{L}{g}}$, where L is the line length and g is the gravity acceleration constant. In Fig. 7, a three-dimensional plot of the sphere motion is shown as a function of time. The red color corresponds to the oscillatory movement of the sphere as a function of time. Blue, yellow, and green colors represent the projection in the different planes.

V. CONCLUSION

Combining active incoherent signal illumination, Fourier domain signal sampling, and element-level digital processing, millimeter-wave imaging with speeds more than 26 times faster than current millimeter-wave imaging approaches has been achieved [23]. Experimental images of point-like reflecting targets were obtained at 652 fps, using a new parallel data acquisition and image formation approach that minimizes latencies. While these targets clearly demonstrate the feasibility of obtaining very high speed millimeter-wave imagery, the specularity of many objects at millimeter-wave frequencies may give rise to additional complexities such as speckle that may need to be addressed while imaging complex targets such as contraband. Nonetheless, the work herein represents a significant leap in the current state of the art of millimeter-wave imaging, and opens the possibilities for the adoption of an emerging imaging modality in a wide range of scientific and commercial applications.

ACKNOWLEDGMENT

The authors would like to thank Brian Wright from Michigan State University for his help with the experimental setup and the antenna fabrication.

REFERENCES

- [1] C. S. Ruf, C. T. Swift, A. B. Tanner, and D. M. L. Vine, "Interferometric synthetic aperture microwave radiometry for the remote sensing of the earth," *IEEE Trans. Geosci. Remote Sens.*, vol. 26, no. 5, pp. 597-611, 1988.
- [2] M. Ruegg, E. Meier and D. Nuesch, "Vibration and Rotation in Millimeter-Wave SAR," *IEEE Trans. Geosci. Remote Sens.*, vol. 45, no. 2, pp. 293-304, Feb. 2007.

- [3] J. A. Nanzer, Microwave and Millimeter-Wave Remote Sensing for Security Applications, Norwood, MA, USA: Artech House, 2012.
- [4] R. Appleby and R. N. Anderton, "Millimeter-Wave and Submillimeter-Wave Imaging for Security and Surveillance," *Proc. IEEE*, vol. 95, no. 8, pp. 1683-1690, Aug. 2007
- [5] Vehicular anticollision radar system for driving in the fog, by P. A. Paoletti, Sep. 3 1991, US Patent 5,045,856.
- [6] D. M. Sheen, D. L. McMakin, and T. E. Hall, "Three-dimensional millimeter-wave imaging for concealed weapon detection," *IEEE Trans. Microw. Theory Techn.*, vol. 49, no. 9, pp. 1581-1592, 2001.
- [7] E. J. Bond, X. Li, S. C. Hagness, and B. D. V. Veen, "Microwave imaging via space-time beamforming for early detection of breast cancer," *IEEE Trans. Antennas Propag.*, vol. 51, no. 8, pp. 1690-1705, 2003
- [8] N. K. Nikolova, "Microwave Imaging for Breast Cancer," IEEE Microw. Mag., vol. 12, no. 7, pp. 78-94, Dec. 2011
- [9] S. Mukherjee, L. Udpa, S. Udpa, and E. J. Rothwell, "Target localization using microwave time-reversal mirror in reflection mode," *IEEE Trans. Antennas Propag.*, vol. 65, no. 2, pp. 820-828, 2017.
- [10] F. Zidane, et al., "Nondestructive control of fruit quality via millimeter waves and classification techniques: Investigations in the automated health monitoring of fruits," *IEEE Antennas Propag. Mag.*, vol. 62, no. 5, pp. 43-54, 2020.
- [11] J. Nadakuduti, Genda Chen, and R. Zoughi, "Semiempirical electromagnetic modeling of crack detection and sizing in cement-based materials using near-field microwave methods," *IEEE Trans. Instrum. Meas.*, vol. 55, no. 2, pp. 588-597, 2006.
- [12] E. C. Fear, J. Bourqui, C. Curtis, D. Mew, B. Docktor, and C. Romano, "Microwave breast imaging with a monostatic radar-based system: A study of application to patients," *IEEE Trans. Microw. Theory Techn.*, vol. 61, no. 5, pp. 2119–2128, 2013.
- [13] P. C. Theofanopoulos, M. Sakr, and G. C. Trichopoulos, "Multistatic terahertz imaging using the radon transform," *IEEE Trans. Antennas Propag.*, vol. 67, no. 4, pp. 2700–2709, 2019.
- [14] R. C. Hansen, *Phased Array Antennas*, John Wiley and Sons, 2002.
- [15] S. H. Talisa, K. W. O'Haver, T. M. Comberiate, M. D. Sharp, and O. F. Somerlock, "Benefits of digital phased array radars," *Proc. IEEE*, vol. 104, no. 3, pp. 530–543, 2016.
- [16] J. Hunt, et al. "Metamaterial apertures for computational imaging," Science, vol. 339, no. 6117, pp. 310–313, 2013.
- [17] T. Sleasman, et al., "Single-frequency microwave imaging with dynamic metasurface apertures," J. Opt. Soc. Am. B, vol. 34, no. 8, pp. 1713–1726, 2017.
- [18] L. Yujiri, M. Shoucri, and P. Moffa, "Passive millimeter wave imaging," *IEEE Microw. Mag.*, vol. 4, no. 3, pp. 39–50, 2003.
- [19] S. Abid, C. Decroze, M. Mouhamadou, and T. Fromenteze, "Enhancing millimeter-wave computational interferometric imaging," *IEEE Access*, vol. 8, pp. 101416–101425, 2020.
- [20] A. V. Diebold, M. F. Imani, T. Fromenteze, D. L. Marks, and D. R. Smith, "Passive microwave spectral imaging with dynamic metasurface apertures," *Optica*, vol. 7, no. 5, pp. 527–536, 2020.
- [21] A. R. Thompson, J. M. Moran, and G. W. Swenson, *Interferometry and Synthesis in Radio Astronomy*, John Wiley and Sons, 2001.
- [22] M. Born and E. Wolf, Principles of optics, Cambridge Univ. Pr., 1999.
- [23] N. A. Salmon, et al., "First video rate imagery from a 32-channel 22-GHz aperture synthesis passive millimetre wave imager," in Proc. SPIE Eur. Security + Defence, Millim. Wave, Terahertz Sens. Technol. IV, pp. 8188, no. 05, 2011.
- [24] I. P. Theron, E. K. Walton, and S. Gunawan, "Compact range radar cross-section measurements using a noise radar," *IEEE Trans. Antennas Propag.*, vol. 46, no. 9, pp. 1285–1288, Sep. 1998.
- [25] R. M. Narayanan and M. Dawood, "Doppler estimation using a coherent ultrawide-band random noise radar," *IEEE Trans. Antennas Propag.*, vol. 48, no. 6, pp. 868-878, June 2000.
- [26] F. D. Palo, G. Galati, G. Pavan, C. Wasserzier, and K. Savci, "Introduction to Noise Radar and Its Waveforms," *Sensors*, vol. 20, no. 18, p. 5187, Sep. 2020.
- [27] S. Vakalis and J. A. Nanzer, "Microwave imaging using noise signals," IEEE Trans. Microw. Theory Techn., vol. 66, no. 12, pp. 5842–5851, 2018.
- [28] S. Vakalis, L. Gong, Y. He, J. Papapolymerou, and J. A. Nanzer, "Experimental demonstration and calibration of a 16-element active incoherent millimeter-wave imaging array," *IEEE Trans. Microw. The*ory Techn., vol. 68, no. 9, pp. 3804–3813, 2020.





- [29] A. Moreira, P. Prats-Iraola, M. Younis, G. Krieger, I. Hajnsek and K. P. Papathanassiou, "A tutorial on synthetic aperture radar," *IEEE Trans. Geosci. Remote Sens.*, vol. 1, no. 1, pp. 6-43, March 2013.
- [30] S. Vakalis and J. A. Nanzer, "A digital interferometric array with active noise illumination for millimeter-wave imaging at 13.7 fps," in 2020 IEEE/MTT-S International Microwave Symposium (IMS), pp. 1141–1144, 2020.
- [31] J. N. Gollubet al., "Large Metasurface Aperture for Millimeter Wave Computational Imaging at the Human-Scale," *Scientific Reports*, vol. 7, no. 1, 42650, 2017.
- [32] S. Vakalis and J. A. Nanzer, "Analysis of array sparsity in active incoherent microwave imaging," *IEEE Geosci. Remote Sens. Lett.*, vol. 17, no. 1, pp. 57–61, 2020.
- [33] S. Vakalis and J. A. Nanzer, "Analysis of element failures in active incoherent microwave imaging arrays using noise signals," *IEEE Microw. Wireless Compon. Lett.*, vol. 29, no. 2, pp. 161–163, 2019.
- [34] J. Garnier and G. Papanicolaou, "Passive sensor imaging using cross correlations of noisy signals in a scattering medium," SIAM J. Imaging Sci., vol. 2, pp. 396–437, 2009.
- [35] S. Vakalis, D. Chen, and J. A. Nanzer, "Toward space-time incoherent transmitter design for millimeter-wave imaging," *IEEE Antennas Wireless Propag. Lett.*, vol. 19, no. 9, pp. 1471-1475, 2020.
- [36] L. Yujiri, et al., "Passive millimeter-wave camera," Proc. SPIE, vol. 3064, pp. 3064 3064 8, 1997.
- [37] J. Drewes and R. P. Daly, "Design of a high-resolution passive millimeter-wavelength camera for security applications," *Proc. SPIE*, vol. 7309, pp. 7309 7309 12, 2009.
- [38] L. Cohen, *Time-frequency analysis: theory and applications*, Prentice-Hall, Inc., USA,1995.
- [39] J. A. Nanzer, "Millimeter-wave interferometric imaging sensors," in SENSORS, pp. 1–4,2013.
- [40] A. B. Tanner et al., "Initial Results of the Geostationary Synthetic Thinned Array Radiometer (GeoSTAR) Demonstrator Instrument," *IEEE Trans. Geosci. Remote Sens.*, vol. 45, no. 7, pp. 1947-1957, 2007.
- [41] https://www.dropbox.com/s/wngpc9adjpzysfd/Mmwave_Imaging_ 652fps.mp4?dl=0
- [42] A. Chambolle, "An algorithm for total variation minimization and applications," J. Math. Imag. Vision, vol. 20, 2004.



STAVROS VAKALIS (Student Member, IEEE) received the Diploma degree in electrical and computer engineering from National Technical University of Athens, Athens, Greece in 2017 and the M.S. degree in electrical and computer engineering from Michigan State University, East Lansing, MI, USA in 2020. He is currently pursuing the Ph.D. degree in electrical engineering at Michigan State University. His current research interests include wireless microwave and millimeter-wave systems,

millimeter-wave imaging, antenna arrays, radar and signal processing.

Mr. Vakalis received the Gerondelis Foundation Graduate Scholarship in 2019, the IEEE Microwave Theory and Techniques Society (IEEE MTT-S) Graduate Fellowship Award in 2021, and an URSI Young Scientist Award in 2021. He was the recipient of the Second Place Awards of both the Student Paper Competition and the Student Design Competition at the 2020 IEEE International Symposium on Antennas and Propagation, and the 2020-21 Fitch H. Beach Award for outstanding research in the College of Engineering, Michigan State University (Honorable Mention). He is a member of the IEEE Microwave Theory and Techniques Society and the IEEE Antennas and Propagation Society. He is currently serving as a reviewer for the IEEE Transactions on Microwave Theory and Techniques, the IEEE Journal of Electromagnetics, RF and Microwaves in Medicine and Biology, the IEEE Transactions on Antennas and Propagation, and the IEEE Geoscience and Remote Sensing Letters.



DANIEL CHEN (Student Member, IEEE) received the B.S. degree in electrical engineering from Michigan State University, East Lansing, MI, USA, in 2015. He is currently pursuing the Ph.D. degree in electrical and computer engineering at Michigan State University, East Lansing, MI, USA. His current research interests include wireless microwave and millimeter-wave systems, antenna arrays, radars and signal processing.



JEFFREY A. NANZER (Senior Member, IEEE) received the B.S. degrees in electrical engineering and in computer engineering from Michigan State University, East Lansing, MI, USA, in 2003, and the M.S. and Ph.D. degrees in electrical engineering from The University of Texas at Austin, Austin, TX, USA, in 2005 and 2008, respectively.

From 2008 to 2009, he was a Post-Doctoral Fellow with Applied Research Laboratories, University of Texas at Austin, where he was involved

in designing electrically small HF antennas and communication systems. From 2009 to 2016, he was with The Johns Hopkins University Applied Physics Laboratory, Laurel, MD, USA, where he created and led the Advanced Microwave and Millimeter-Wave Technology Section. In 2016, he joined the Department of Electrical and Computer Engineering, Michigan State University, where he is currently a Dennis P. Nyquist Assistant Professor. He has authored or co-authored more than 150 refereed journal and conference papers, authored Microwave and Millimeter-Wave Remote Sensing for Security Applications (Artech House, 2012), and co-authored the chapter "Photonics-Enabled Millimeter-Wave Wireless Systems" in Wireless Transceiver Circuits (Taylor & Francis, 2015). His current research interests include distributed arrays, radar and remote sensing, antennas, electromagnetics, and microwave photonics.

Dr. Nanzer is a member of the IEEE Antennas and Propagation Society Education Committee and the USNC/URSI Commission B. He was a founding member and the First Treasurer of the IEEE APS/ MTT-S Central Texas Chapter. He served as the Vice Chair for the IEEE Antenna Standards Committee from 2013 to 2015. He was the Chair of the Microwave Systems Technical Committee (MTT-16), IEEE Microwave Theory and Techniques Society from 2016 to 2018. He was a recipient of the Outstanding Young Engineer Award from the IEEE Microwave Theory and Techniques Society in 2019, the DARPA Director's Fellowship in 2019, the National Science Foundation (NSF) CAREER Award in 2018, the DARPA Young Faculty Award in 2017, and the JHU/APL Outstanding Professional Book Award in 2012. He is currently an Associate Editor of the IEEE TRANSACTIONS ON ANTENNAS AND PROPAGATION.